DEVELOPMENT OF IMPROVED INELASTIC DISPLACEMENT PREDICTION EQUATIONS FOR THE SEISMIC DESIGN OF HYBRID SYSTEMS

J.L. Ceballos C.[1] and T.J. Sullivan[2]

SUMMARY

The use of hybrid joints to provide pre-cast concrete and timber structures with ductile response and self-centering capability is becoming increasingly popular in New Zealand, as is evident by the increasing number of building solutions that incorporate the technology as well as the design provisions for hybrid systems currently included in the New Zealand Concrete standard. This paper raises some issues with the current code approach to estimate the inelastic seismic displacement demand on hybrid systems. The work then presents the results of a series of non-linear time history analyses of single degree of freedom (SDOF) systems characterised by the flag-shaped hysteretic rule, in order to identify a general, improved expression for the equivalent viscous damping of hybrid systems. The new equivalent viscous damping expression is expected to provide more reliable control of inelastic displacement demands for hybrid systems design used Displacement-Based Design (DBD) procedures. In addition, the last part of the paper also discusses how the findings in the paper could be utilised to provide improved control of displacement demands when hybrid systems are designed using force-based procedures.

Keywords: hybrid; inelastic displacement; Equivalent viscous damping; Flag-shaped hysteretic behaviour; Direct Displacement-Based Design.

INTRODUCTION

Hybrid joint systems have been developed over the past two decades (see [1] to [7]) in order to provide both pre-cast concrete and, more recently, timber structures with ductile response and self-centering capabilities. For a detailed background to the technology available for RC systems see [8]. The potential of hybrid systems is now fairly well recognised in New Zealand, as is evident by the increasing number of building solutions ([9], [10]) that incorporate the technology as well as the design provisions included in Appendix B of NZS3101 [11] and the Press Design Handbook [8]. Joints of hybrid pre-cast concrete systems resist seismic actions through a combination of pre-stressing (that provides self-centering capacity) and yielding non-prestressed reinforcement or other special devices that provide energy dissipation. The hysteretic moment-rotation response of hybrid systems can be idealised by the flag-shaped hysteretic response illustrated in Figure 1.

The hysteretic loop reported in Figure 1 is an idealization of the actual response, as experimental results (see, for example, [12] to [17]) show that in reality the loops will be curved and may not go perfectly through the origin. However, the simplified hysteretic shape defined in Figure 1 is considered to contain the main characteristics that are needed to examine the non-linear dynamic response of hybrid systems and experimental data shows that this idealization can provide acceptable results [18], [19], [20].

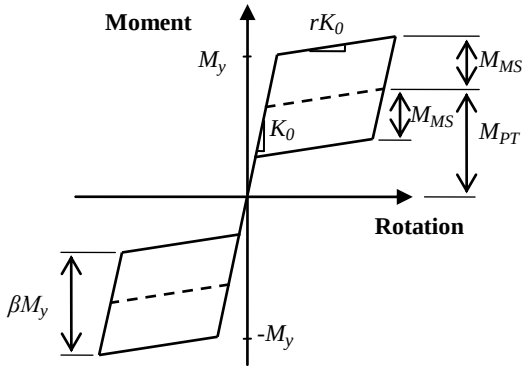

Figure 1: Flag-shaped hysteretic response of hybrid structures.

Given that the purpose of this paper will be to provide engineers with new design relationships that permit, in a simplified fashion, improved inelastic displacement predictions for hybrid systems, the flag-shape model is used in this work. Nevertheless, since a flag-shape hysteresis loop is only an approximate idealisation to the real hysteretic behaviour of hybrid systems, for detailed non-linear time-history analyses of specific hybrid systems refined alternative models should be considered.

The seismic behaviour of hybrid systems is considerably influenced by the relative proportions of resistance offered by pre-stressing and dampers. To characterise the relative proportions of joint resistance, the factor λ defined by Equation (1) is often used and this is equal to the ratio of the

[1] *Masters Graduate, ROSE School, IUSS Pavia, Pavia, Italy*

[2] *Assistant Professor, Department of Structure Mechanics, University of Pavia, Pavia, Italy (member)*

prestressing bending resistance, M_{PT}, to the dampers (mild steel bars for traditional RC hybrid systems) bending resistance contribution, M_{MS}, (see Figure 1):

$$\lambda = \frac{M_{PT}}{M_{MS}} \quad (1)$$

Hence, with increasing lambda factor, λ, the flag shape tends to be ''thinner'' and the energy dissipated in a loop decreases. A similar parameter used to gauge the proportions of resistance is the β factor, also shown in Figure 1 and related to the λ factor by Equation (2):

$$\beta = \frac{2}{\lambda + 1} \quad (2)$$

This definition is useful since the β factor is input in Ruaumoko [21] for Non-Linear Time-History (NLTH) analyses of hybrid systems with flag-shaped hysteresis. Note that in addition to the λ factor, another hysteretic characteristic that can have a significant effect on the non-linear dynamic response of hybrid systems is the post-yield stiffness ratio, *r*.

In this paper, current expressions for the inelastic displacement prediction of hybrid systems will be reviewed and an improved means of predicting the inelastic displacement of hybrid systems with account for their different hysteretic characteristics will be proposed, based on the results of non-linear time-history analyses.

INELASTIC DISPLACEMENT ESTIMATES OF HYBRID SYSTEMS ACCORDING TO THE NEW ZEALAND STANDARD

A key parameter for good seismic performance of a building is the peak deformation (displacement or peak storey drift) that the building experiences during an earthquake. In fact, the strength and stiffness of hybrid systems is often governed by the need to satisfy code defined deformation limits, such as those defined in Section 7 of the New Zealand Earthquake Loadings Standard (NZS1170 part 5 [22]), possibly modified in line with the recommendations of NZS3101. In practice, the New Zealand Concrete Structures Standard (NZS3101-2006 [11]) permits the design of hybrid systems through either force-based or displacement-based design procedures.

For displacement-based design of pre-cast hybrid systems, NZS3101 permits the equivalent viscous damping to be interpolated between a value of 5% (corresponding to an unbonded connection) and an expression for a monolithic frame system, leading to the hybrid equivalent viscous damping expression of Equation (3):

$$\xi_{NZS\,3101} = 0.05 + \frac{0.30}{\lambda + 1}\left(1 - \frac{1}{\sqrt{\mu}}\right) \quad (3)$$

where μ is the displacement ductility demand. Note that this paper will show that this simplified formulation for the equivalent viscous damping of hybrid systems is not accurate and alternative expressions should be used.

Equivalent viscous damping expressions of the form given by Eq.(3) can be used to control the inelastic displacement of the hybrid system in line with the Direct DBD approach (Priestley *et al*. [23]) or the capacity spectrum approach (Freeman; [24], [25]). In these approaches the elastic response spectra are scaled to the system equivalent viscous damping value by using damping spectral reduction expressions such as that given in Equation (4), recommended by Priestley *et al*. [23]) and included in the 1993 version of the Eurocode 8 [26]:

$$\eta_{EC8} = \left(\frac{0.07}{0.02 + \xi_{eq}}\right)^{0.5} \quad (4)$$

where ξ_{eq} is the equivalent viscous damping, which is defined by the sum of elastic and hysteretic damping.

Note that other damping spectral reduction expressions have been proposed in the literature, as will be discussed further later in the paper. Figure 2 shows an elastic response spectrum and a highly damped spectrum obtained by factoring the spectral ordinates by the η factor obtained from Equation (4).

The spectra are plotted on axes of acceleration versus displacement by pairing the spectral acceleration at a given period with the spectral displacement at the same period and then plotting these coordinates as a series of points on acceleration-displacement axes. By plotting the spectra in this format, the non-linear force-displacement response of a SDOF hybrid system can be superimposed, as shown in Figure 2, noting that the system acceleration can be multiplied by mass to obtain an equivalent force value (which is likely to be more familiar to designers).

In Direct DBD, the designer identifies the target displacement for the system and then reads off a required effective period from a highly-damped displacement response spectrum, which is then used to obtain a required effective stiffness and design base shear (see [23]).

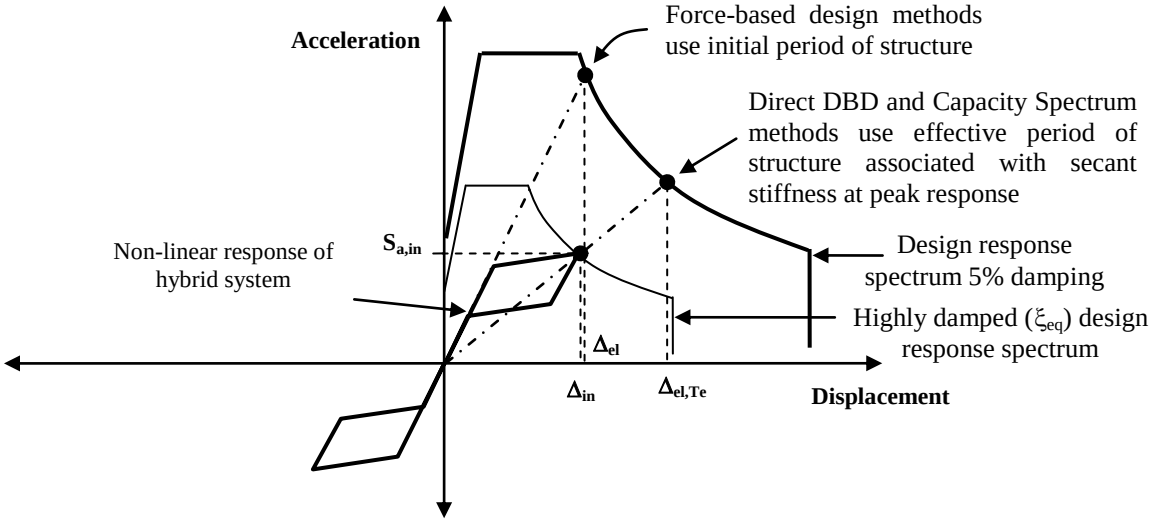

Figure 2: Means of identifying the inelastic displacement according to displacement-based and force-based design approaches.

This is equivalent to identifying the target displacement (Δ_{in}) along the horizontal axis of Figure 2, and then finding the required acceleration (which multiplied by mass gives the required system strength) from the intersection point with the highly damped spectrum. This approach, and in particular the use of the effective stiffness, stems from the substitute structure concepts introduced by Gulkan and Sozen [27], and Shibata and Sozen [28].

The same concepts are incorporated within the capacity spectrum approach [24] but, as pointed out by Priestley *et al*. [23], the Capacity Spectrum approach is formulated as an assessment procedure since the designer should first develop and then plot the acceleration-displacement curve for the system, which suggests that the designer already knows the system strength. Equivalent viscous damping values for each point along the acceleration-displacement pushover curve are then established through Equation (3), and then the expected inelastic response is found by indentifying the highly damped spectrum that intersects the acceleration-displacement curve at the same value of equivalent viscous damping (for further details see [24] or [25]).

Irrespective of whether designers prefer to use the equivalent viscous damping within a Direct DBD or a Capacity Spectrum approach, it is clear that by including the equivalent viscous damping expression of Equation (3) in NZS3101 [11], designers are provided with a rational means of controlling the inelastic displacements of hybrid systems.

On the other hand, neither Appendix B of the NZ Concrete Standard nor the NZ Earthquake Loadings Standard [22] appear to provide special guidance on how the inelastic displacements should be controlled when designing hybrid systems using a force-based design method such as the equivalent lateral force method or the modal response spectrum method. The Commentary to the NZ Concrete Standard does make reference to the fib Bulletin 27 [29] which argues that force-based design can be used for hybrid systems provided that the force-reduction factor accounts for the joint hysteretic characteristics. For inelastic displacement prediction, the fib Bulletin 27 recommends that for medium and long period systems the inelastic displacements be estimated through the equal displacement rule which implies that the inelastic displacement of the system is expected to be approximately equal to the displacement of an equivalent elastic system with the same initial period of vibration. Similarly, if a designer wishes to estimate the inelastic displacement of a hybrid system according to NZS1170 part 5, then one would assume that the same approach used for other structural systems is adopted; the displacements obtained from an inelastic spectrum are amplified by the ductility factor, μ, in line with the equal displacement approximation (when building period is such that $k_\mu = \mu$).

The equal displacement concept can also be illustrated with reference to Figure 2. In the equal displacement approach, the initial period is first used to identify the elastic spectral displacement, Δ_{el}, (and note that this is equivalent to the displacement obtained from inelastic design spectra of NZS1170 amplified by the ductility, μ). The equal displacement approach then states that the inelastic displacement, Δ_{in}, should be approximately equal to the elastic spectral displacement, Δ_{el}, and so the elastic displacement is used to verify whether or not deformation limits are satisfied.

The equal-displacement approximation appears to stem principally from the work of Velestos and Newmark [30] and Riddell and Newmark [31]. In their work, the peak inelastic response of elasto-plastic, bi-linear and stiffness degrading SDOF systems, determined through NLTH analyses, was compared against that predicted using the initial period with elastic response spectra and the general "equal-displacement" trend was observed for medium and long period structures. As reported by Priestley *et al.* [23] amongst others, NLTH analysis results have shown that the equal displacement approximation is non-conservative for flag-shaped hysteretic systems subject to medium and high ductility demands, particularly if tangent-stiffness based elastic damping is assumed. As a consequence, designers following the New Zealand Standard recommendations for force-based design of hybrid systems are likely to be unwittingly underestimating the peak displacements (and therefore the damage) that the buildings will undergo. This suggests that until a new inelastic to elastic spectral displacement relationship is specified for hybrid systems, engineers should be advised to use an equivalent viscous damping approach for the design of such systems.

Returning to the recommendation to use Equation (3) for the equivalent viscous damping of hybrid systems, it will be shown that this expression is also considered to be of limited accuracy owing to its simplicity. The expression assumes that the equivalent viscous damping can be interpolated from upper and lower bound expressions for equivalent viscous damping of completely different hysteretic shapes. Other equivalent viscous damping expressions having been developed specifically hybrid systems, as will be discussed in more detail in the next section, but the expressions are not generalised to account for a wide range of hysteretic characteristics that one could expect for hybrid systems. Given the apparent importance of equivalent viscous damping expressions for the design of hybrid systems, this work will present the results of a series of NLTH analyses that will be used to highlight the performance of the current expression in NZS 3101 and propose an improved expression for design. The work will also then review the results of the NLTH analyses in order to indicate how a compatible force-based design approach might be formulated.

A REVIEW OF EXISTING EXPRESSIONS FOR THE EQUIVALENT VISCOUS DAMPING OF HYBRID SYSTEMS

As stated in the previous section, there are a number of different equivalent viscous damping expressions proposed in the literature. Through a series on NLTH analyses using a set of artificial accelerograms, Grant *et al.* [32] developed Equation (5) for hybrid systems with $\lambda = 4.7$:

$$\xi_{eq,Grant} = 0.05 + 0.186\left(\frac{\mu - 1}{\mu\pi}\right) \quad (5)$$

In a similar manner, Pennucci *et al.* [33] also used the results of NLTH analyses to set an expression (Equation 6) for the equivalent viscous damping of hybrid systems with $\lambda = 1.25$:

$$\xi_{eq,Pennucci} = 0.05 + 0.524\left(\frac{\mu - 1}{\mu\pi}\right) \quad (6)$$

Recently, Mpampatsikos *et al.* [34] also used NLTH analyses to develop the following more general expression (Equation 7) for the equivalent viscous damping of hybrid systems:

$$\xi_{eq,Mpampatsikos} = 0.05 + \frac{2.348}{(\lambda + 3.901)}\left(\frac{\mu - 1}{\mu\pi}\right) \quad (7)$$

However, note that while this expression does cover a range of λ factors, it does not take into account the influence of the post-yield stiffness factor r.

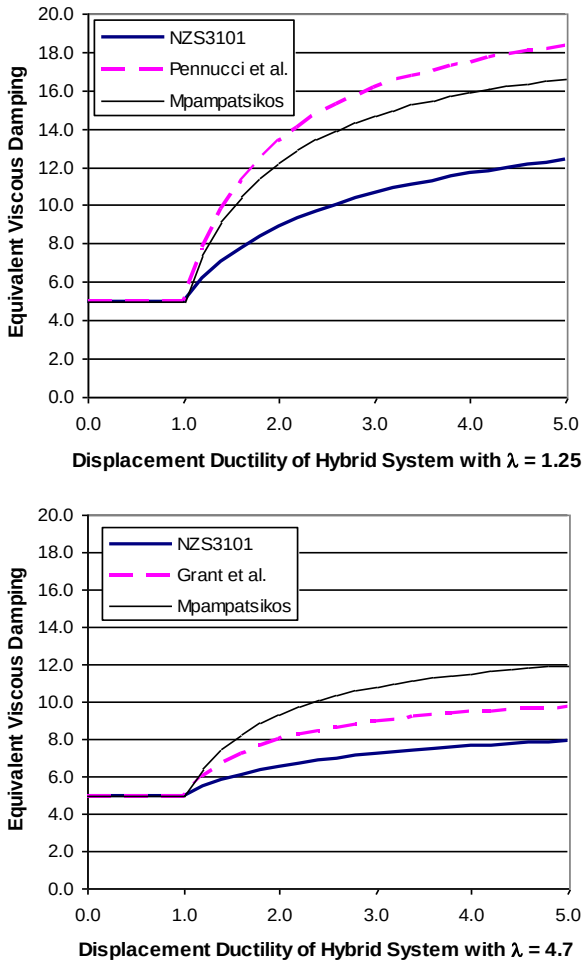

Figure 3: Comparison of different equivalent viscous damping expressions proposed for hybrid systems in the literature: (a) hybrid systems with λ = 1.25 and (b) hybrid systems with λ = 4.7.

Figure 3 compares the equivalent viscous damping obtained by the different expressions with that predicted by the current expression in the New Zealand Standard, for lambda values of λ = 1.25 and λ = 4.7. Interestingly there are significant differences between the existing expressions for the equivalent viscous damping. However, it is comforting to note that the NZS3101 expression appears to provide the most conservative estimates of equivalent viscous damping between the different expressions.

Given the uncertainty raised by the comparison of existing equivalent viscous damping expressions in Figure 3, this work will consider a large number of hybrid systems characterised by different lambda factors, λ, and the post-yield stiffness ratios, r, as part of a NLTH analysis campaign aimed at developing a general improved expression for the equivalent viscous damping of hybrid structures and thereby better control of displacements and damage.

METHODOLOGY USED TO DEVELOP NEW EQUIVALENT VISCOUS DAMPING EXPRESSION

With the aim of developing expressions for estimation of equivalent viscous damping of hybrid concrete structures, to be used in a displacement based design procedure, this section studies the analytical response of different SDOF systems with flag shaped hysteresis behaviour, simulating the inelastic response of this kind of hybrid structures under different ground motions records.

Procedure

The scope of the procedure is to determine the value of equivalent viscous damping to be applied to an equivalent elastic system with a given effective period (based on the secant stiffness to maximum displacement response) such that the highly damped linear system predicts the same displacement as an inelastic system with flag shaped hysteresis rule that, when subject to non-linear time-history analysis (NLTHA), develops the same effective period to develop for a given level of ductility.

The final objective of the procedure is to develop equations that define the equivalent viscous damping factor to be used in the DDBD of hybrid structures, as a function of the ductility demand. The flow diagram for the proposed method is shown in Figure 5.

The methodology for the equivalent viscous damping estimation can be described step by step as follows:

Step 1: Initially, select the parameters that describe the SDOF system, hence an effective period (T_{eff}), an effective mass (m_{eff}) and a ductility level (μ) are selected.

Step 2: Select the flag-shaped hysteresis rule for the inelastic behaviour the SDOF system, defining the hysteretic parameters; the shape factor β and the post-yield stiffness factor r.

Step 3: Select an accelerogram, from the ground motion set presented in the Table 1.

Step 4: Define an ultimate displacement (Δ_u). The ultimate displacement is defined arbitrarily since it is only a target displacement that will be reached during the non linear time history analysis by an iterative process as indicated in Steps 5 to 8.

Step 5: For the given SDOF system, the initial stiffness (K_o) and yield force (F_y), are computed considering the selected ultimate displacement (Δ_u), effective mass (m_{eff}), effective period (T_{eff}) and the ductility (μ) as follows.

Effective stiffness:

$$K_{eff} = \frac{4\pi^2 m_{eff}}{T_{eff}^2} \tag{8}$$

Maximum force:

$$F_{\max} = K_{eff}\Delta_u \tag{9}$$

Yield force:

$$F_y = \frac{K_{eff}\Delta_u}{\left[1 + r\left(\mu - 1\right)\right]} \tag{10}$$

Yield displacement:

$$\Delta_y = \frac{\Delta_u}{\mu} \tag{11}$$

Step 6: Run non-linear time-history analysis of a SDOF system with yield strength F_y from Equation (10), yield displacement Δ_y from Equation (11) and hysteretic parameters matching those in step 1. Get the maximum displacement

response (Δ_{max}) from the hysteresis behaviour that comes out from the NLTHA.

Step 7: Compare the maximum displacement (Δ_{max}) obtained from NLTHA with the ultimate displacement defined initially (Δ_u).

Step 8: If the difference between displacements from Step 7. are negligible, within a tolerance of 3%, continue with step 9, otherwise, scale the accelerogram and return to step 6 running non-linear time-history analysis with the scaled ground motion record, until the excitation generates a displacement within the specified tolerance. In other words, this step identifies the intensity of the ground motion that would cause the target displacement and ductility to develop.

Note that the process is principally dependent only on the period, hence it is irrelevant what mass is selected, because the period will control the stiffness and strength required. Any combination of mass and stiffness (and F_y / *Mass*) that gives the same period will give equivalent results.

Step 9: Compute the displacement response spectrum for the scaled accelerogram considering damping values from 0% to 30%. Find the displacement response spectra for which the point defined by T_{eff} and Δ_u, matches closest the response spectra, as shown in Figure 4. That chosen spectra corresponds to a specific damping value that defines the equivalent viscous damping for the SDOF system under study. Hence, it is found the equivalent viscous damping for the given SDOF system.

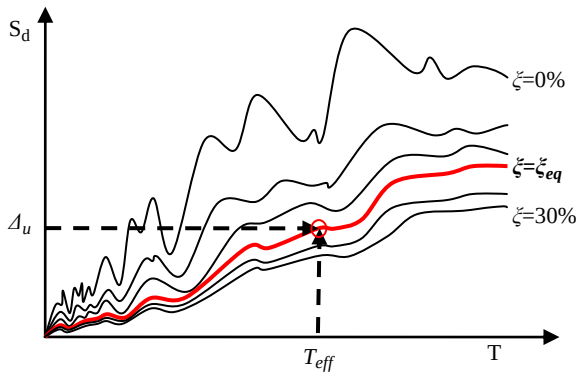

Figure 4: Step 9 - Spectral matching to obtain EVD values.

The displacement spectra for all the different values of damping, mentioned before, were computed using the program for processing strong-motion data, SeismoSignal [35], getting the elastic displacement response spectra for a given accelerogram and damping.

Accelerograms and displacement spectra

Accelerograms

For the present study, two kinds of strong ground motion records were used, representing both far-field and near-fault events. All records were taken from the PEER online strong ground motion database, from the Pacific Earthquake Engineering Research Center, University of California at Berkeley [36].

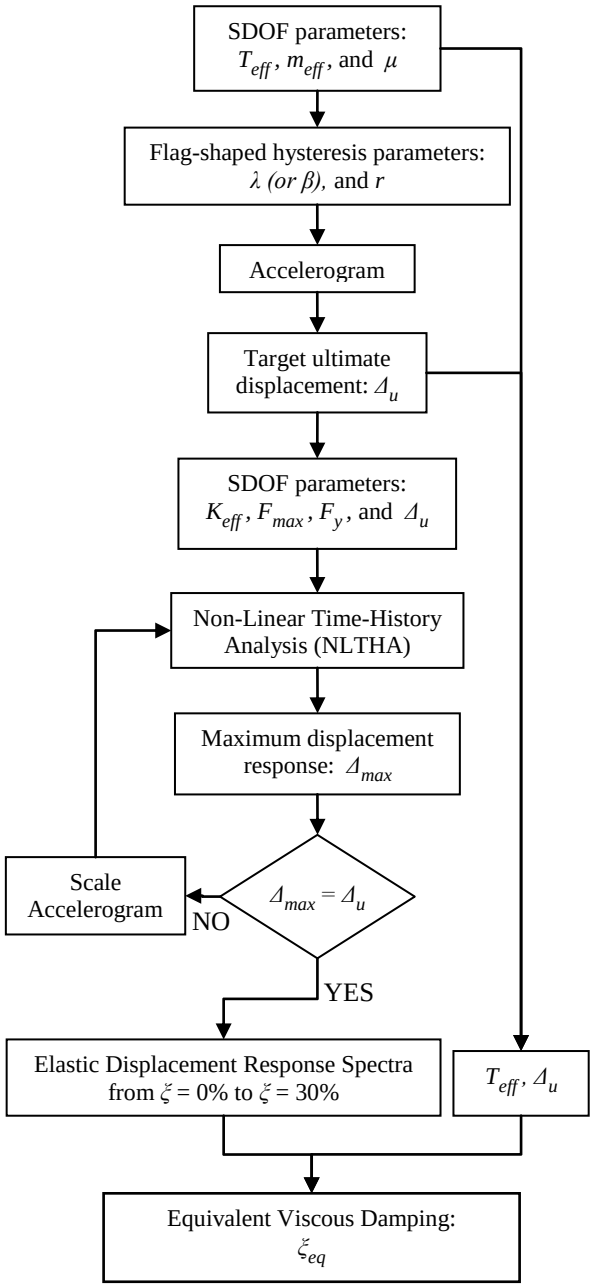

Figure 5: Flow diagram for the EVD estimation procedure.

The first suite of earthquakes is an ensemble of 20 historical 'far-field' strong ground motion records. These records were related to soil types C or D (NEHRP categories), with hypocentre depth ranging between 13 and 25 km, and were generated by earthquakes of moment magnitude, M_w, ranging from 6.7 to 7.3. The second suite of earthquakes is an ensemble of 10 historical near-fault earthquake records, selected based on its PGV/PGA ratio (at least 0.09 ms^{-1}/ms^{-2}) and distance from fault (less than 10 km) (Kam *et al.* [37]; Christopoulos *et al.* [38]). It is important to say that key characteristics of near-field events are a low number of cycles and high velocity pulses which can yield larger displacement and ductility demands on the structures as reported in [37] where one can also find additional information about some of the selected records, which were used for previous studies.

Records considered in the study are not necessarily spectrum compatible and this characteristic is not a requirement in order to obtain a wide range of results representing the influence of all different parameters involved in ground motion records.

Table 1. Selected ground motions.

Label	Earthquake Name / Station Name	Magnitude	ClstD (km)
EQ1	Imperial Valley-06 / El Centro Array #7	6.53	0.6
EQ2	Imperial Valley-06 / Delta	6.53	22
EQ3	Imperial Valley-06 / Superstition Mtn Camera	6.53	24.6
EQ4	Superstition Hills-02 / Brawley Airport	6.54	17
EQ5	Superstition Hills-02 / El Centro Imp. Co. Cent	6.54	18.2
EQ6	Erzican, Turkey / Erzincan	6.69	4.4
EQ7	Northridge-01 / Sylmar- live View Med FF	6.69	5.3
EQ8	Northridge-01 / Newhall - Fire Sta	6.69	5.9
EQ9	Northridge-01 / Rinaldi Receiving Sta	6.69	6.5
EQ10	Northridge-01 / N.Hollywood-Coldwater Can	6.69	12.5
EQ11	Northridge-01 / Canoga Park - Topanga Can	6.69	14.7
EQ12	Northridge-01 / Glendale - Las Palmas	6.69	22.2
EQ13	Northridge-01 / LA - UCLA Grounds	6.69	22.5
EQ14	Northridge-01 / LA - Hollywood Stor FF	6.69	24
EQ15	Northridge-01 / Santa Monica City Hall	6.69	26.5
EQ16	Northridge-01 / LA - Saturn St	6.69	27
EQ17	Kobe, Japan / KJMA	6.9	1
EQ18	Loma Prieta / Los Gatos - Lexington Dam	6.93	5
EQ19	Loma Prieta / Saratoga - W Valley Coll.	6.93	9.3
EQ20	Loma Prieta / Gilroy Array #3	6.93	12.8
EQ21	Loma Prieta / WAHO	6.93	17.5
EQ22	Loma Prieta / UCSC	6.93	18.5
EQ23	Loma Prieta / Hollister Diff. Array	6.93	24.8
EQ24	Cape Mendocino / Petrolia	7.01	8.2
EQ25	Cape Mendocino / Rio Dell Overpass - FF	7.01	14.3
EQ26	Landers / Lucerne	7.28	2.2
EQ27	Landers / Coolwater	7.28	19.7
EQ28	Landers / Desert Hot Springs	7.28	21.8
EQ29	Landers / Yermo Fire Station	7.28	23.6
EQ30	Tabas, Iran / Tabas	7.35	2.1

Shape of displacement spectra

Reviewing the shape of the displacement spectra for each of the records listed in Table 1, it was noted that half of the records did not possess linearly increasing spectral displacement demands over the period range of interest to this study. Work by Pennucci *et al.* [39] has shown that spectral shape is important for the development of inelastic displacement prediction equations. Consequently, from the 30 records initially selected, only the 15 records that possess linearly increasing displacement spectra were finally used for calibration of the new equivalent viscous damping expression in this work. See [40] for further details and discussion.

Modelling

Using the program Ruaumoko [21], SDOF systems are modelled considering zero length translational springs with flag shaped hysteresis loop, running non-linear time history analysis. Dynamic inelastic time history analyses were conducted using the Newmark constant average acceleration, with a lumped mass matrix, and tangent stiffness Rayleigh damping model with 5% of critical damping.

For the hysteretic behaviour of the SDOF systems, the inelastic response is represented by the flag shaped hysteresis rule. The flag shape factor (β), initial stiffness (K_o), yield force (F_y), post yield stiffness factor (r), effective mass (m_{eff}), and the ductility (μ) are inputs according to the case under study.

The main variables for this study are the post-yield stiffness factor (r) and the flag shape factor (β), which can be expressed also in terms of (λ). In order to see the influence of the variation of such hysteresis parameters on the inelastic displacements, values of r between 0.05 and 0.20, and values of l between 1.0 and 9.0 were examined, as shown in Table 2.

Table 2. Considered post-yield stiffness, flag shape factors, effective period and ductility values.

Parameter	Considered values
r	0.05, 0.10, 0.15, 0.20
λ (β)	1.0 (*1.0*), 1.5 (*0.8*), 2.0 (*0.67*), 3.0 (*0.5*), 5.1 (*0.33*), 9.0 (*0.2*)
T_{eff} $[s]$	0.5, 1.0, 1.5, 2.0, 2.5, 3.0, 3.5, 4.0
μ	1.5, 2.0, 3.0, 4.0, 5.0, 6.0

Also note that for the parametric study it is important to analyse the behaviour of different SDOF systems, and for this reason it was considered necessary to introduce variables that describe the SDOF characteristics, such as the effective period (T_{eff}) and the ductility (μ). The range of these values considered in the work are also listed in Table 2.

In order to illustrate the modelling of Non-Linear Time History Analysis, Figure 6 shows the hysteretic behaviour of different SDOF systems subjected to some of the ground motions records previously described. Each subplot in Figure 6 corresponds to the inelastic behaviour of a SDOF system with effective period (T_{eff}), ductility (μ), and characterized by a hysteretic rule with flag shape factor (β) and post yield stiffness factor r, subjected to a given earthquake.

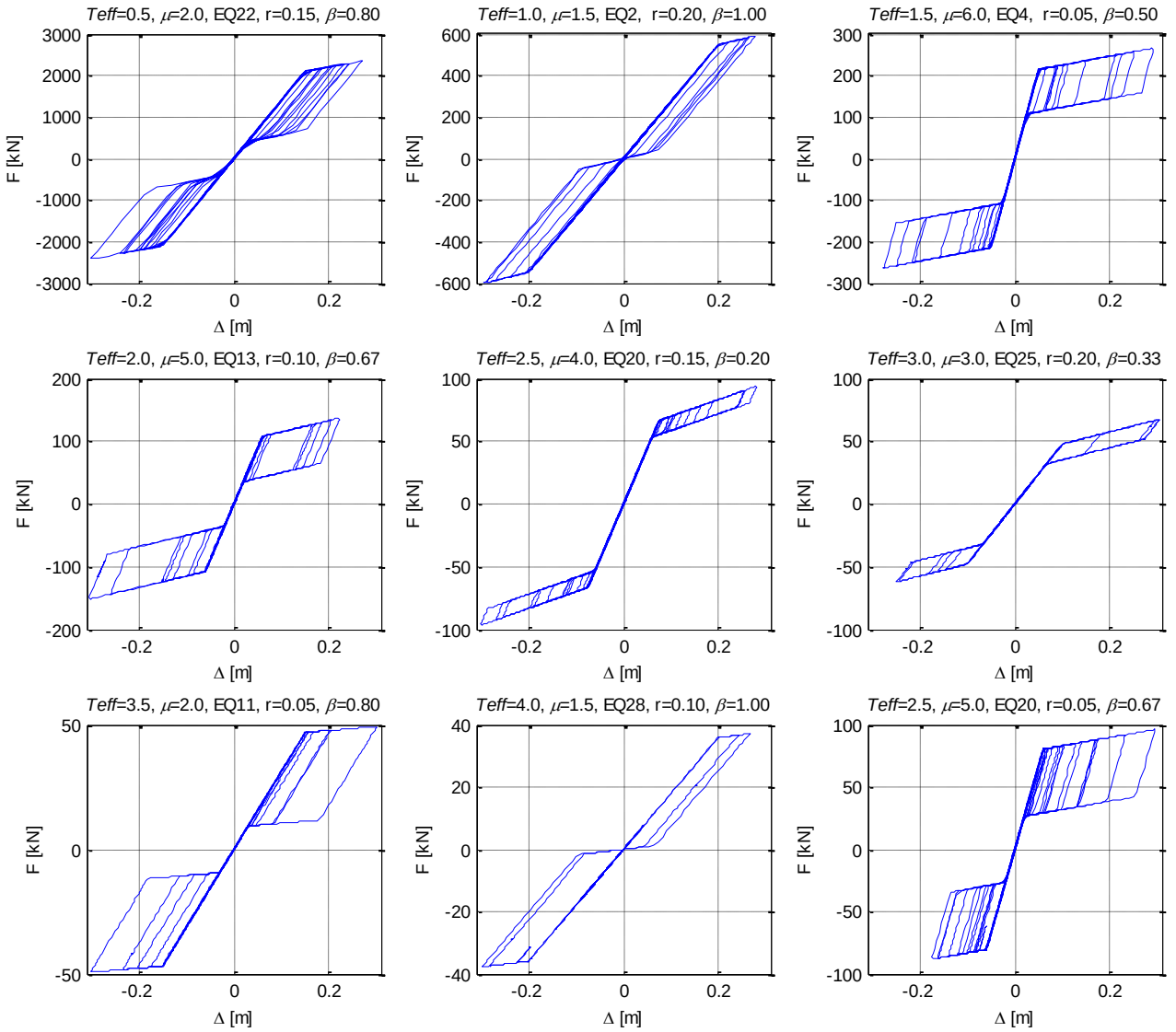

Figure 6: Examples of Hysteretic loops, for different SDOF systems and ground motions.

RESULTS OF EQUIVALENT VISCOUS DAMPING STUDY

Applying the procedure described in the previous section to the range of hybrid SDOF systems identified in Table 2, a large quantity of results are obtained that provide equivalent viscous damping (EVD) data points. In order to interpret the results, it is necessary to organize the data and results to find the curves that best fit the EVD tendency. The data fitting procedure is explained and illustrated below.

NLTHA results and processing procedure

Having obtained EVD results for a large number of cases, it is important to understand the influence of the variables on the EVD. However, because the amount of results is very large, it is necessary to compute average values of the hysteretic damping, for each studied effective period and ductility, distinguishing between the post-yield stiffness factor (r) and flag shape factor (β).

Every selected SDOF system, with specific effective period, ductility and hysteretic parameters, was analysed under all considered ground motion records, providing a range of equivalent viscous damping values for each SDOF system due to the differences between the accelerograms. Hence, to condense the results for a set of calculated values, the mean and the coefficient of variation (C.O.V.) of the EVD were calculated. Consequently, for a SDOF with effective period (T_{eff}), ductility (μ) and hysteretic parameters (r and β), the average equivalent viscous damping is obtained.

Additionally, it was seen that spikes in the elastic response spectra cause a large dispersion in the apparent EVD values. At the same time, it is expected that the variation of the results due to such spikes is random, with the approach sometimes overestimating the damping and sometimes underestimating the damping, such that the average of the equivalent viscous damping values should be representative, justifying the use of average values to overcome this issue.

Figure 7 to Figure 10 show the behaviour and tendency of the EVD for a given value of post-yield stiffness ratio, r and flag shape depth factor, β in terms of ductility and effective period. Note that the EVD values shown take the average results from the set of accelerograms applied to each SDOF system.

The results illustrate that the damping depends on the flag depth (β, or λ if preferred) and the post-yield stiffness ratio. There is also a tendency for the damping to increase with the ductility, but not very greatly, and at short effective periods the EVD tends to be higher suggesting some period dependency. However, for periods from 1.0s to 4.0s the EVD values hover around the same level. These trends were considered in setting a new EVD expression.

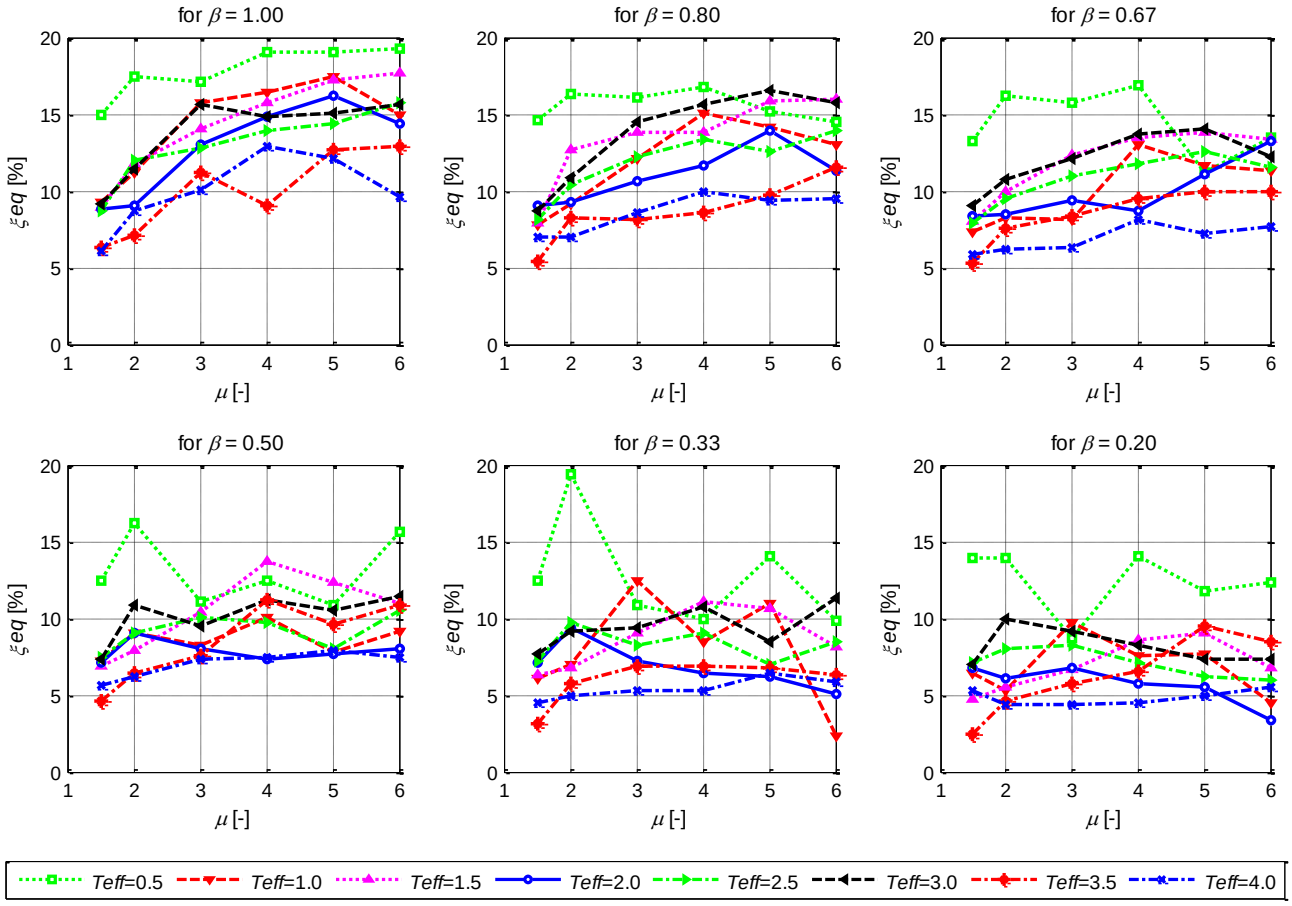

Figure 7: Average Equivalent Viscous Damping for r = 0.05.

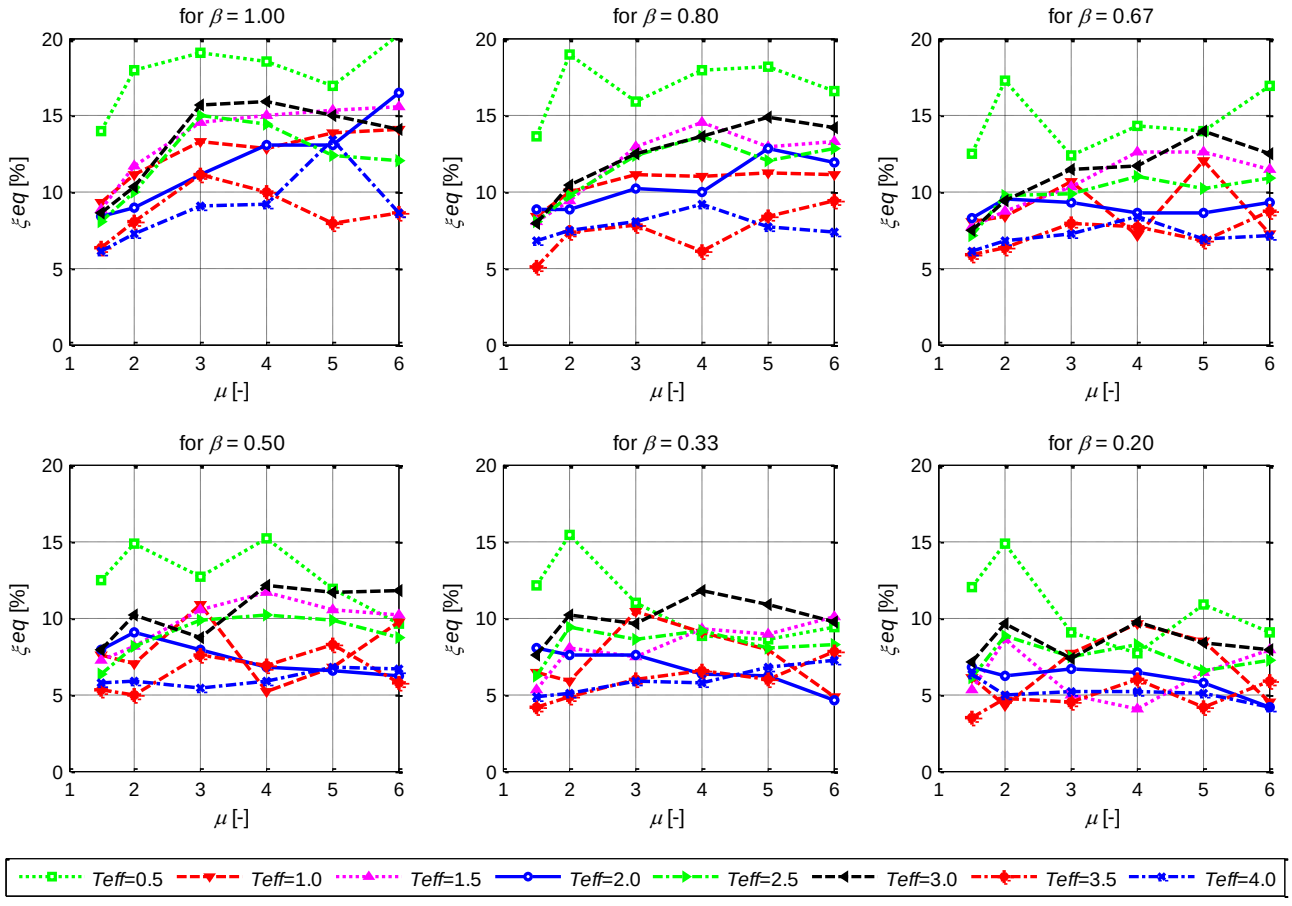

Figure 8: Average Equivalent Viscous Damping for r = 0.10.

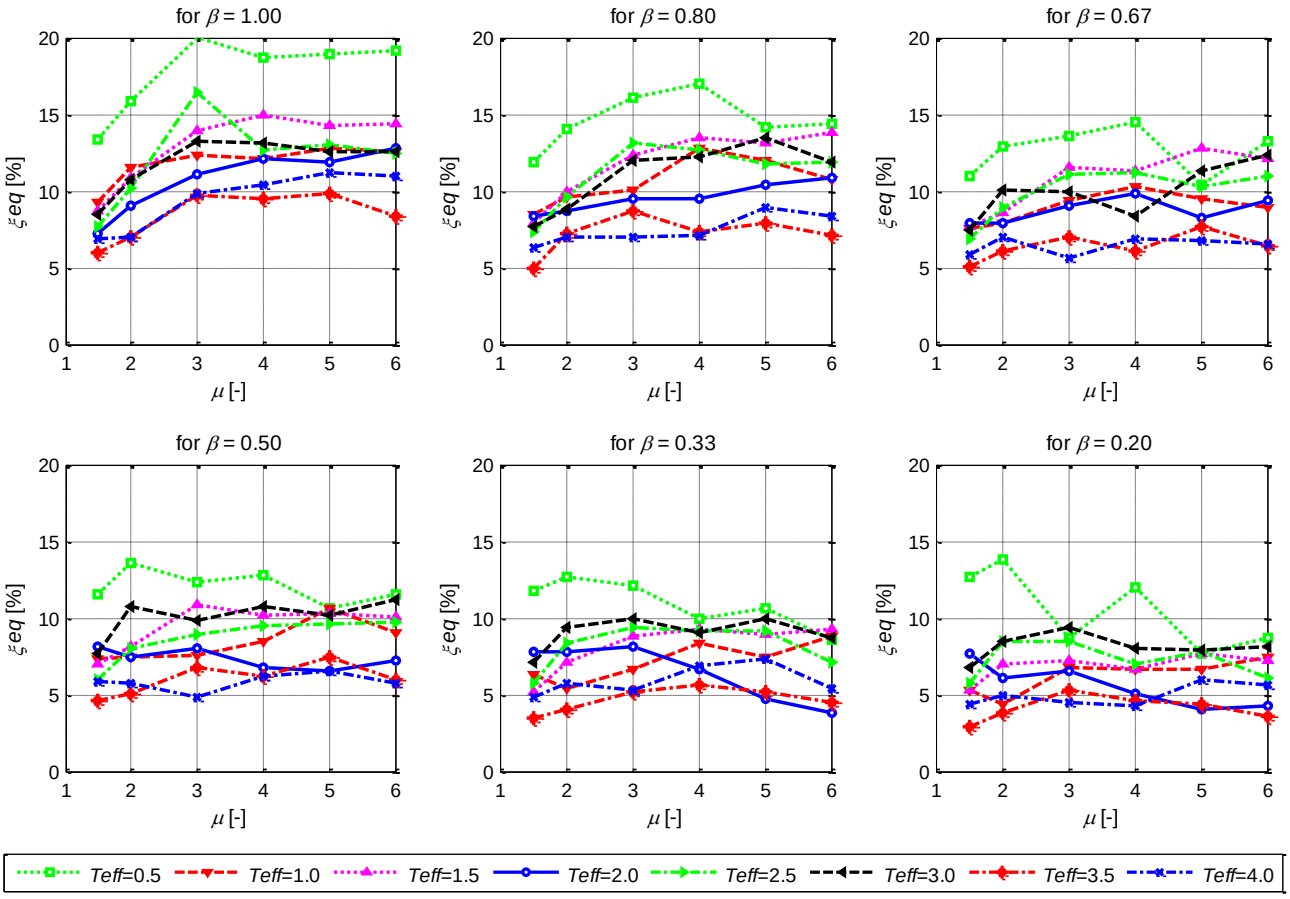

Figure 9: Average Equivalent Viscous Damping for r = 0.15.

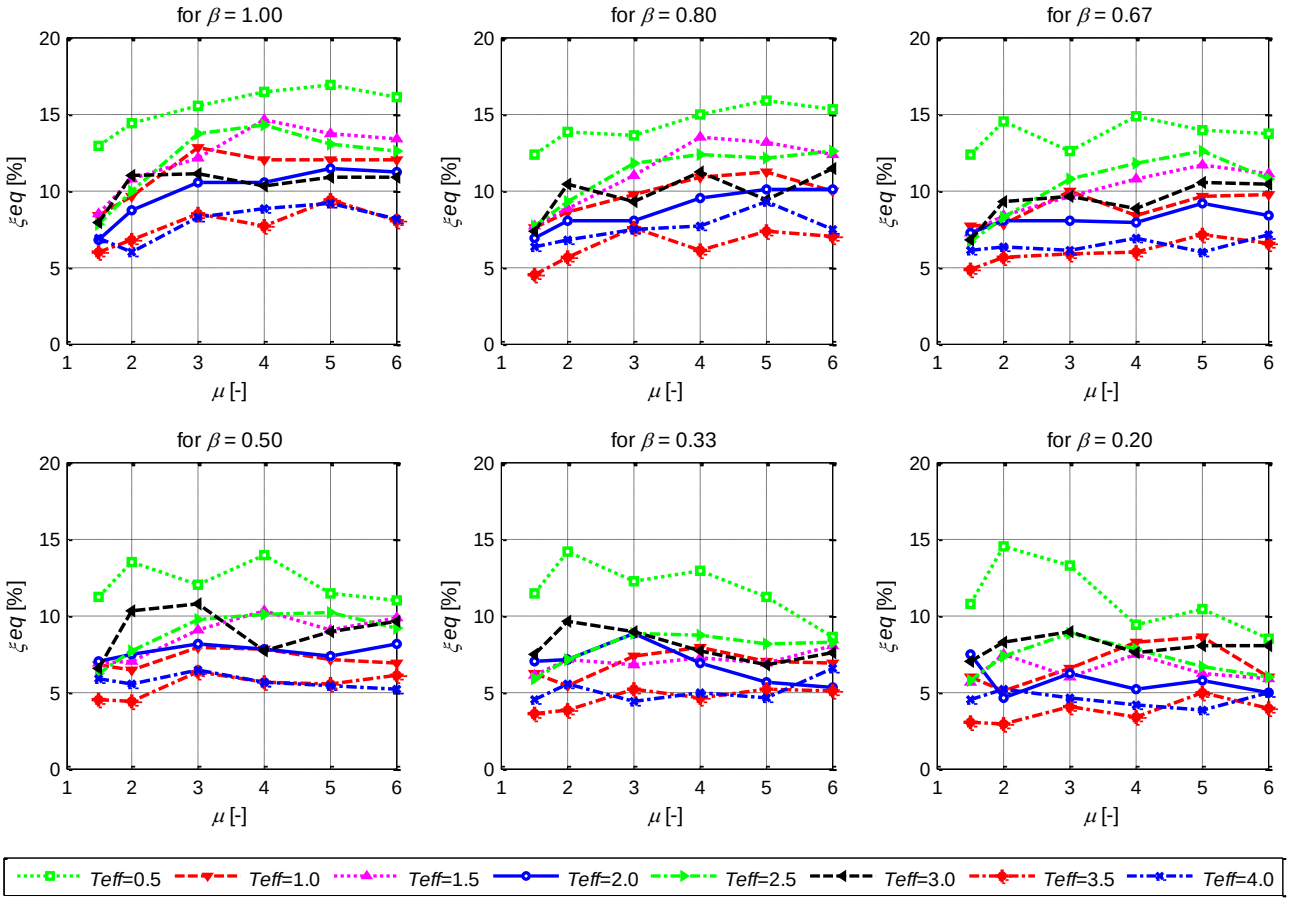

Figure 10: Average Equivalent Viscous Damping for r = 0.20.

Fitting of EVD expressions to NLTHA results

In order to develop an expression for the equivalent viscous damping that keeps a similar form of that used by Grant *et al*. [32] and Pennucci *et al*. [33] but with the ability to consider different λ and r values directly as per the Jacobsen formulation (refer [23]), the following form of Equivalent Viscous Damping expression should be developed:

$$\xi_{eq} = 0.05 + \frac{C}{(\lambda+1)(1+r(\mu-1))}\left(\frac{\mu-1}{\mu\pi}\right) \qquad (12)$$

where C is a constant that is used to obtain the best fit with the NLTHA results.

Following this process for the NLTHA results presented in the previous section, it was found that the coefficient C can be expressed as a function of λ and the post-yield stiffness ratio, r, as shown in Equation (13).

$$\xi_{eq} = 0.05 + \frac{(0.324\lambda+1)(1-r)}{(\lambda+1)(1+r(\mu-1))}\left(\frac{\mu-1}{\mu\pi}\right) \qquad (13)$$

Readers interested in reviewing the complete procedure used to fit Equation (13) to the NLTH analysis results should refer to [40].

Finally, 3D plots are elaborated as a function of the flag-shaped factor, the ductility and the post-yield stiffness factor, where Equation (13) is plotted for four different cases of r, as is shown in Figure 11.

USING THE NEW EQUIVALENT VISCOUS DAMPING EXPRESSION TO CONTROL INELASTIC DISPLACEMENTS

Clearly, the main objective of establishing the new equivalent viscous damping expression (Equation 13) is to provide practitioners with an improved means of controlling inelastic displacements. To this extent, recall that in the displacement-based design procedures described earlier, inelastic displacements are related to the elastic response spectra by scaling the elastic response spectra using a damping spectral reduction equation such as that reported earlier in Equation (4). The relationship between elastic design spectra and inelastic displacements is therefore dependent on both the equivalent viscous damping and the damping spectral reduction equation. Note that there are actually a large number of damping spectral reduction equations proposed in the literature. For example, in the 2003 revision to Eurocode 8 [26] Equation (4) was replaced by Equation (14),

$$\eta = \left(\frac{0.10}{0.05+\xi}\right)^{0.5} \qquad (14)$$

Work by Faccioli *et al*. [41] has indicated that this expression represents the effect of viscous damping on the elastic spectra of real earthquake records better than Equation (4) that was included in the earlier version of Eurocode 8. Priestley *et al*. [23] recommend, however, that when designing non-linear systems with the equivalent viscous damping expressions presented in their book, Equation (4) should be used to scale the design response spectrum as a function of damping, even if the spectra of real records at the site may scale according to Equation (14) or another damping reduction equation.

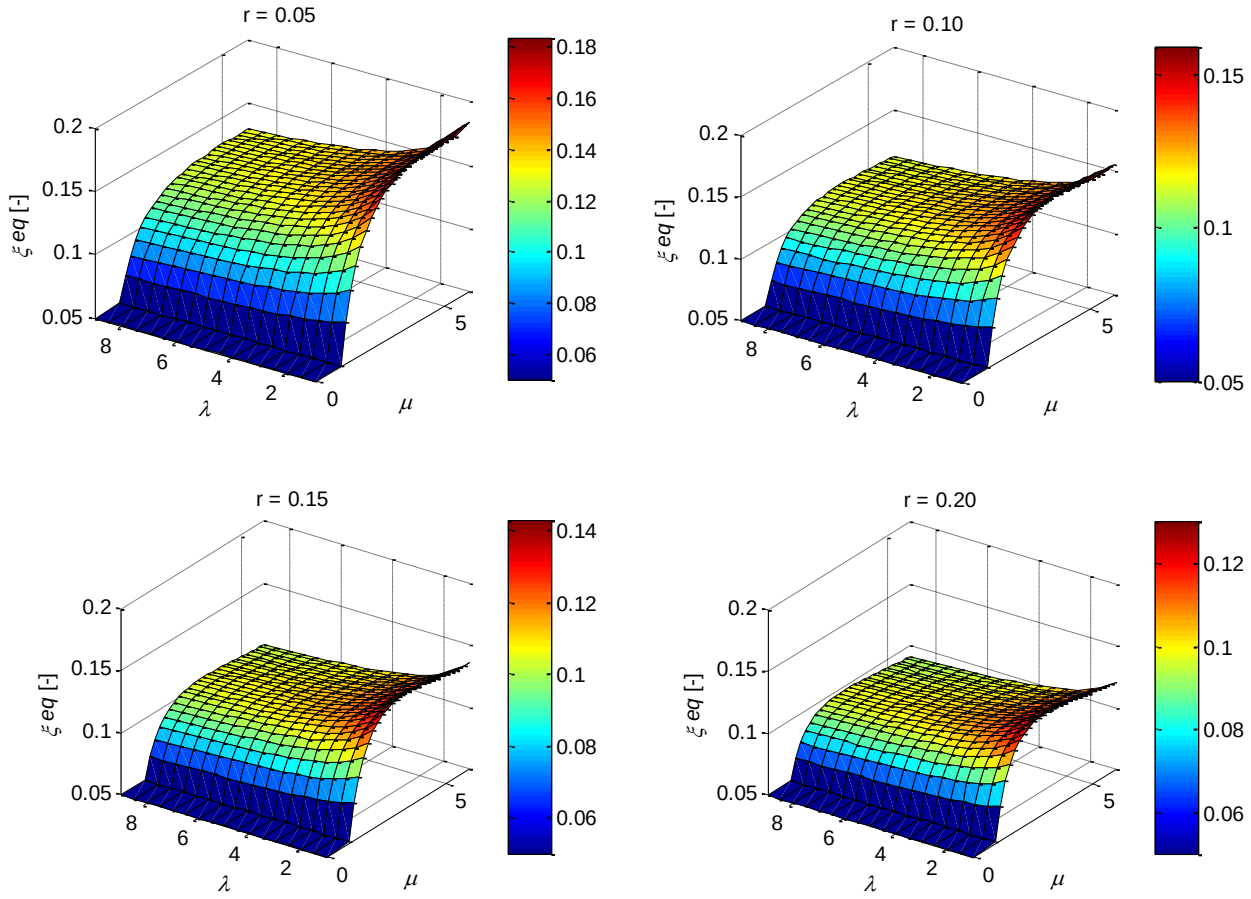

Figure 11: 3D plots for the proposed EVD expression for different post-yield factors.

Recently, Pennucci *et al*. [39] have obtained analytical results that support this recommendation of Priestley *et al*. [23]. Pennucci *et al.* found that equivalent viscous damping expressions for non-linear systems, calibrated to the results of NLTH analyses, should be used in combination with the spectral damping reduction expression that characterises the records used for the NLTH analyses. As already stated, this finding supports the recommendation of Priestley *et al*. [23]. Another way of interpreting the finding of Pennucci *et al*. [39] is that the η factor itself should be directly a function of the hysteretic characteristics and expressions for η can therefore be formed by incorporating equivalent viscous damping expressions directly into damping reduction equations.

As reported earlier, 15 real earthquake records were used in this work to run the non-linear time-history analyses and calibrate the new equivalent viscous damping expression proposed for hybrid systems. By considering the elastic spectra at a range of viscous damping levels, it is found that the damping spectral reduction equation that best characterises the 15 selected records is given by:

$$\eta = \left(\frac{0.115}{0.065 + \xi} \right)^{0.5} \tag{15}$$

Inserting Equation (13) into Equation (15), gives:

$$\eta = \left(\frac{1}{1 + \frac{(0.9\lambda + 2.8)(1 - r)}{(\lambda + 1)(1 + r(\mu - 1))} \left(1 - \frac{1}{\mu}\right)} \right)^{0.5} \tag{16}$$

Also note that since the spectral reduction factor has been calibrated to match the maximum inelastic displacements obtained from non-linear time-history analyses, the reduction factor can be considered as the ratio of the inelastic displacement to the elastic spectral displacement at the effective period, $\Delta_{el,Te}$ (see Figure 2), as stated in Equation (17):

$$\eta = \frac{\Delta_{in}}{\Delta_{el,Te}} \tag{17}$$

This relationship helps emphasise the usefulness of Equation (16) for the control of inelastic displacements. The benefit of developing Equation (16) is that it permits the spectral displacement reduction factor to be calculated directly as a function of the hysteretic characteristics and ductility demand. Moreover, however, the process of inserting the equivalent viscous damping expression into the damping reduction equation permits a more appropriate comparison of existing equivalent viscous damping expressions.

Figure 12 presents a comparison of existing expressions for the spectral displacement reduction factor, η, with the new expression given by Equation (16). Note that in developing the curves from the Pennucci *et al*. [33] and Mpampasikos *et al.* [34] equivalent viscous damping expressions, the elastic damping expression of Equation (14) was used since this best matched the real records they utilised for their NLTH analyses. In contrast, in order to develop the curve shown for Grant *et al*. [32], the elastic damping expression of Equation (4) was used since this best matched the artificial records they utilised for their NLTH analyses. The results of Figure 12 are very encouraging. It can be seen that three independent studies, conducted using different sets of accelerograms, all provided very similar expressions for the spectral displacement reduction factor for hybrid systems. The good correlation between the new and existing expressions somewhat validates the new Equivalent viscous damping expression in Equation (13) or, if preferred, the direct spectral displacement reduction expression given by Equation (16). These new expressions could therefore be used as part of a displacement-based design approach to obtain more reliable control of the inelastic displacement demands on hybrid systems.

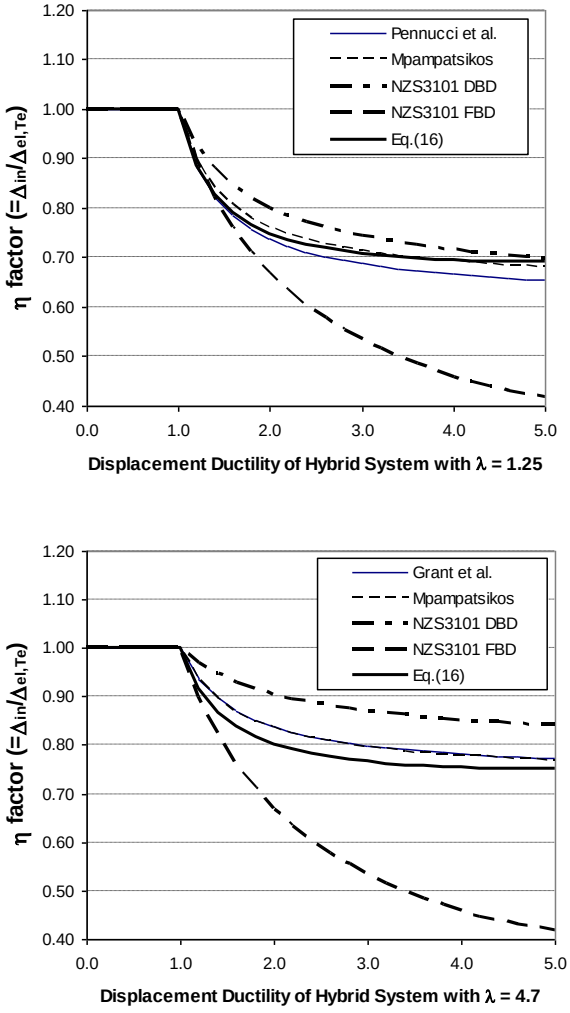

Figure 12: Comparison of developed η factor with the expressions presented in the literature: (a) hybrid systems with λ =1.25 and (b) hybrid systems with λ = 4.7.

APPLICATION OF NEW KNOWLEDGE WITHIN FORCE-BASED DESIGN OF HYBRID SYSTEMS

As discussed in the introduction, the New Zealand Standard NZS3101 permits the design of RC hybrid systems using either force-based or displacement-based design procedures. This research has developed Equation (13) and Equation (16) for the improved prediction of inelastic displacement demands of hybrid systems within a displacement-based design context. Equation (16) can also be useful for the prediction of inelastic displacements as part of a force-based design approach, as will be shown here.

Firstly, note that with knowledge of the expected system ductility demand, μ, and post-yield stiffness ratio, r, (refer

Figure 1), the force-based designer can compute the η value given by Equation (16). However, this may appear of limited use since the displacement reduction factor is typically used with the effective period spectral displacement demands and not those of the initial period, which is used in force-based design. In order to account for this, the designer can calculate the effective period, T_{eff}, using the initial period, T_i, as shown in Equation (18):

$$T_{eff} = T_i \sqrt{\frac{\mu}{1+r(\mu-1)}} \tag{18}$$

The elastic spectral acceleration at the initial period and at the effective period should then be obtained as shown in Figure 13.

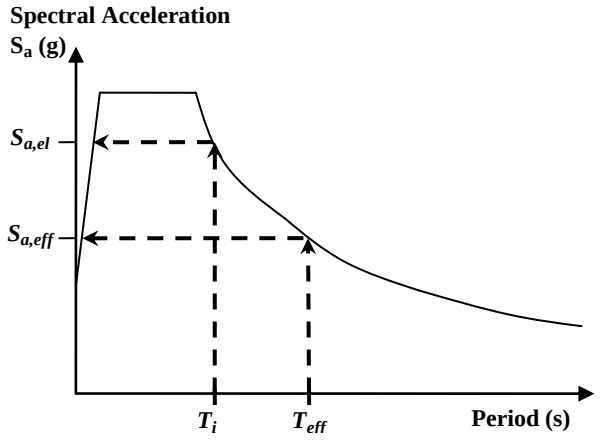

Figure 13: Use of elastic spectral acceleration response spectrum within a force-based design approach.

At this stage the force-based designer should compute the elastic displacements, Δ_{el}, expected on the structure (refer Figure 2) by using the building initial period, T_i, and structural analysis for actions associated with an unreduced design response spectrum (i.e. elastic spectral acceleration $S_{a,el}$ in Figure 13). The inelastic displacements can then be predicted from the elastic displacements through Equation (19):

$$\Delta_{in} = \frac{S_{a,eff}}{S_{a,el}} \eta \frac{\mu}{[1+r(\mu-1)]} \Delta_{el} \tag{19}$$

Where $S_{a,el}$ is the elastic spectral acceleration for the initial period, $S_{a,eff}$ is the elastic spectral acceleration for the effective period, η is the factor obtained from Equation (16), μ is the system ductility demand and r is the post-yield stiffness ratio (see Figure 1). As such, the findings of this work can also be used to obtain improved inelastic displacement predictions within a force-based design context.

Note that Equation (19) suggests that the relationship between the elastic and inelastic displacement demands is likely to depend on both the period of the structure, the ductility demand and the hysteretic characteristics. By inserting typical values for each of the parameters into Equation (19) one can show that the equal-displacement rule is likely to be very non-conservative at times. Consider, for example, a hybrid system with an initial period of T_i = 0.8s and λ factor = 1.25, an r = 0.05, and a system ductility demand of μ = 4.0. The η for this system would be 0.7 (Equation (16) or Figure 12) and the effective period T_{eff} = 1.5s. With reference to typical response spectra in the loadings standard, one can show $S_{a,eff}$ / $S_{a,el}$ = 0.63. Substituting these values into Equation (19) one finds that the inelastic displacement is expected to be 1.5 times the elastic displacement demand. This process has been repeated for a range of ductility values and the equivalent h factor has then been plotted within Figure 12. It is apparent that inelastic displacement estimates obtained using a FBD approach with the equal displacement rule, in accordance with New Zealand Standards, are non-conservative. In addition, Figure 12 shows that there are large discrepancies between inelastic displacement estimates made using the FBD and DBD approaches. This result indicates that NZ codes may require revision to improve inelastic displacement estimates for hybrid systems, and the expressions provided in this work may be a good alternative to current code recommendations.

Note that while this section has attempted to improve the inelastic displacement estimates that one obtains through force-based design, these modifications cannot overcome other serious shortcomings with force-based design for certain structural systems, identified by Priestley *et al*. [23]. As such, it is recommended that designers use displacement-based design or verify their force-based design solutions with advanced non-linear analyses.

CONCLUSIONS

Hybrid structures can provide an excellent lateral stability system in seismic regions as has been shown in previous research. In an effort to support the use of hybrid technology, this work has reviewed and developed expressions for the prediction of inelastic displacements of hybrid systems. Initially, the paper identifies the different approaches recommended by the New Zealand standards for the estimation of inelastic displacement demands on hybrid systems. It is shown that equivalent viscous damping expressions proposed for displacement-based design appear to be fairly conservative, whereas the equal-displacement rule incorporated within force-based design procedures can be very non-conservative.

In order to provide a simplified but improved means of estimating inelastic displacement demands on hybrid systems this work presents the results of a large series of non-linear time-history (NLTH) analyses which are used to calibrate a general equivalent viscous damping expression for hybrid structures characterised with a flag-shaped hysteretic behaviour. Processing of the NLTH analysis results showed that the hysteretic damping increases when λ decreases, as expected, because for low λ values, the energy dissipation offered by mild steel bars or dampers is greater. It was also shown that the equivalent viscous damping values should be lower for higher values of post-yield stiffness factor r. Note, however, that the hysteresis parameter λ has a larger influence on EVD than the post-yield stiffness factor. As part of the investigation procedure it was found that due to the accelerogram and spectrum characteristics, a large dispersion in the equivalent viscous damping values was obtained with coefficients of variation (COV) in the order of 20% to 60%. However, when comparing the new expression developed in this work for the mean inelastic displacement of hybrid systems with other expressions in the literature it was found that there is excellent correlation, thereby providing partial validation of the new equivalent viscous damping and spectral displacement reduction expressions. Finally, in order to render the findings of this work beneficial for engineers undertaking force-based design, a series of simple transformations are presented in order to assist such designers obtain better inelastic displacement estimates.

REFERENCES

1 Christopoulos, C., Filiatrault, A., Uang, C.M. & Folz, B. (2002). "Post-tensioned Energy Dissipating Connections for Moment Resisting Steel Frames, *ASCE Journal of Structural Engineering* , Vol. **128**, No. 9, pp. 1111-1120.

2 Kim, J. (2002). Behavior of hybrid frames under seismic loading. Ph.D. Thesis, Civil Engineering, University of Washington.

3 Kurama, Y. and Shen, Q., 2004. "Post-tensioned hybrid coupled walls under lateral loads." *J. Struct. Eng*., **130**(2), 2004, pp. 297-309.

4 Palermo A., Pampanin, S., Calvi, G.M. (2005). "Concept and development of Hybrid Systems for Seismic-Resistant Bridges", *Journal of Earthquake Engineering*, Imperial College PRESS, Vol. **9** (6), pp. 899-921

5 Stanton, J. F., Stone, W. C., Cheok, G. S. (1997). "A Hybrid Reinforced Precast Frame for Seismic Regions", *PCI Journal*, Vol. **42**, No. 2, pp. 20-32.

6 Priestley, M.J.N. (1991). Overview of the PRESSS Research Programme, *PCI Journal*, Vol.**36**, No.4, pp.50-57.

7 Priestley, M. J. N., Sritharan, S., Conley, J. R. and Pampanin, S. (1999). "Preliminary results and conclusions from the PRESSS five-story precast concrete test building." *PCI Journal*, **44**(6), pp. 42-67.

8 NZ Concrete Society (2010). *PRESSS design handbook Edited by Stefano Pampanin*, NZ Concrete Society, Auckland, New Zealand

9 Cattanach, A. & Pampanin, S. (2008). "21st century precast: The detailing and manufacture of New Zealand's first multi-storey PRESSS building" *In Proceedings of the 2008 New Zealand concrete industry conference*, 2-4 October, Rotorua, New Zealand.

10 Harington, P. (2011). "The EXPAN Solution: Post-Tensioned Wood System Ready for Anything" In-*Wood Digital*, March 2011, pp.4-7.

11 Standards New Zealand, "NZS 3101:2006, Concrete Structures Standard".

12 Pampanin, S., Amaris, A., Akguzel, U. and Palermo, A. (2006). "Experimental investigation on high-performance jointed ductile connections for precast frames" *Proceedings of First European Conference on Earthquake Engineering and Seismology*, Geneva, Switzerland.

13 Amaris, A., Pampanin, S., Bull, D.K. and Carr, A.J. (2008). "Experimental investigation on a hybrid jointed precast frame with non-tearing floor connections" *Proceedings of NZSEE Conference*.

14 Filiatrault, A., Restrepo, J. and Christopoulos, C. (2004). "Development of self-centering earthquake resisting systems" *Proceedings of 13th Conference on Earthquake Engineering*, Vancouver, B.C., Canada.

15 Marriott, D., Pampanin, S., Bull, D.K. and Palermo, A. (2008). "Dynamic testing of precast, post-tensioned rocking wall systems with alternative dissipating solutions" *Proceedings of NZSEE Conference*.

16 Iqbal, A., Pampanin, S., Buchanan, A., and Palermo, A. (2007). "Improved seismic performance of LVL post-tensioned walls coupled with UFP devices" *Proceedings of 8th Pacific Conference on Earthquake Engineering*, Singapore.

17 Iqbal, A., Pampanin, S., and Buchanan, A. "Seismic behaviour of prestressed timber columns under bi-directional loading" *Department of Civil Engineering, University of Canterbury*, Christchurch, New Zealand.

18 Palermo, A., Pampanin, S. and Carr, A. (2005). "Efficiency of simplified alternative modelling approaches to predict the seismic response of precast concrete hybrid systems" *Proceedings of fib Symposium "Keep Concrete Attractive"*, Budapest, Hungary.

19 Pampanin, S. Amaris, A. and Palermo, A. (2006). "Uni and Bi-directional Quasi Static Tests on Alternative Hybrid Precast Beam Column Joint Subassemblies" *Proceedings of NZSEE Conference*.

20 Pennucci, D. (2008). "Displacement based design of precast walls with additional dampers" *Master thesis*,, European School for Advanced Studies in Reduction of Seismic Risk (ROSE School), University of Pavia, Italy.

21 Carr, A.J. (2005). "Ruaumoko 2D: User Manual", *Computer Program Library*, Department of Civil Engineering, University of Canterbury, Christchurch, New Zealand.

22 Standards New Zealand, "NZS 1170.5:2004, Structural Design Actions, Part 5, Earthquake Actions New Zealand".

23 Priestley, M.J.N., Calvi, G.M., and Kowalsky, M.J. (2007). "Displacement-Based Seismic Design of Structures", *IUSS Press*, Pavia, Italy.

24 Freeman, S.A. (1978). "Prediction of Response of Concrete Buildings to Sever Earthquake Motion" *ACI 1978*; Special Publication SP-55: pp. 589-605.

25 Freeman, S.A. (1998). "The Capacity Spectrum Method as a Tool for Seismic Design" Proc. Of the 11th European Conference of Earthquake Engineering, Sept. 6-11, Paris.

26 CEN (1998). "Eurocode EC8 - Design of structures for earthquake resistance - Part 1: General rules, seismic actions and rules for buildings, prEN-1998-1," Comite Europeen de Normalization, Brussels, Belgium.

27 Gulkan, P. and Sozen, M. (1974). "Inelastic Response of Reinforced Concrete Structures to Earthquake Motions." *ACI Journal*, Vol. **71**, No.12, pp. 604-610.

28 Shibata, A., Sozen, M., (1976). "Substitute Structure Method for Seismic Design in R/C." *Journal of the Structural Division, ASCE*, 102(1), pp. 1-18.

29 International Federation for Structural Concrete (2003). "Seismic design of precast concrete building structures" *fib bulletin 27*, Lausanne.

30 Velestos, R. and Newmark, N.M. (1960). "Effect of Inelastic Behaviour on the Response of Simple Systems to Earthquake Motions" Vol. **2** proceedings of 2nd World Conference on Earthquake Engineering, Japan, pp. II-663 to II-682.

31 Riddell, R. and Newmark, N.M. (1979). "Statistical Analysis of the Response of Nonlinear Systems Subjected to Earthquakes" *University of Illinois Research Report* UILU-ENG 79-2016, 291 pages.

32 Grant, D.N., Blandon, C.A., Priestley, M.J.N. (2005). "Modelling Inelastic Response in Direct Displacement-Based Design", *IUSS Press*, Pavia, Italy.

33 Pennucci, D., Calvi, G.M. and Sullivan T.J. (2008). "Displacement-based design of precast walls with additional dampers" *Journal of Earthquake Engineering*. Vol. **13**, Supplement 1, pp. 40-65.

34 Mpampatsikos, V. (2009). "DDBD of Rocking Walls with Mild Steel Dissipaters" *PhD thesis*, European School for Advanced Studies in Reduction of Seismic Risk (ROSE School), University of Pavia, Italy.

35 SeismoSoft (2009). SeismoSignal – Computer Program and user manual, available online from http://www.seismosoft.com.

36 PEER (2009). Online strong ground motion database. Pacific Earthquake Engineering Research Center, University of California at Berkeley, United States of America.

37 Kam, W.Y., Pampanin, S., Palermo, A. and Carr, A.J. (2006). "Advanced Flag-Shaped systems for high seismic performance" *Proceedings of First European Conference on Earthquake Engineering and Seismology (ECEES)*, Genova, Italy.

38 Christopoulos, C., Filiatrault, A. and Folz, B. (2001). "Seismic response of self-centering hysteretic SDOF systems" *Journal of Earthquake Engineering and Structural Dynamics*. pp. 1131–1150

39 Pennucci, D., Sullivan, T.J., and Calvi, G.M., (2011). "Displacement Reduction Factors for the Design of Medium and Long Period Structures" *Journal of Earthquake Engineering*, Vol. **15**, Supplement 1, pp. 1-29.

40 Ceballos C., J.L. (2010). "Equivalent Viscous Damping Expressions for the Direct Displacement Based Design of Hybrid Structures" ROSE School *Master thesis*, IUSS Pavia, Pavia, Italy.

41 Faccioli, E., Paolucci, R. and Rey, J. (2004). "Displacement Spectra for Long Periods" *Earthquake Spectra*, Vol. **20**, No. 2, pp. 347-376.